RAA 2021 Vol. **21** No. **5**, 120(12pp) doi: 10.1088/1674-4527/21/5/120

http://www.raa-journal.org *http://iopscience.iop.org/raa*

***R**esearch in*
***A**stronomy and*
***A**strophysics*

LO And: an A-subtype contact binary with a very cool third component

Hui-Ping Huang[1], Yun-Xia Yu[1,2], Ting Yu[3], Ke Hu[1,2] and Fu-Yuan Xiang[1,2]

[1] Key Laboratory of Stars and Interstellar Medium, Xiangtan University, Xiangtan 411105, China; *yu.sunny@126.com, hooke@xtu.edu.cn, fyxiang@xtu.edu.cn*
[2] Department of Physics, Xiangtan University, Xiangtan 411105, China
[3] Shanghai Astronomical Observatory, Chinese Academy of Sciences, Shanghai 200030, China

Received 2020 September 27; accepted 2020 December 15

Abstract Despite the intensive investigations since the discovery of LO And approximately 60 yr ago, its evolutionary status and subtype are still a matter of controversy. By simultaneously modeling the radial-velocity curves and new light curves with the `Wilson-Devinney` code, we present new geometric, photometric and absolute parameters for this system. The simultaneous solution suggests that LO And is an A-subtype contact binary with a contact degree of 32.4%. The absolute parameters are modified to become $M_1 = 1.409\ M_\odot$, $M_2 = 0.449\ M_\odot$, $R_1 = 1.36\ R_\odot$ and $R_2 = 0.83\ R_\odot$. From our observations and data from surveys, we determined 334 eclipse timings. The $O - C$ diagram, constructed from the new eclipse timings and those reported in the literature, reveals a secular increase and a cyclic variation in its orbital period. The former is caused by conservative mass transfer from the secondary component with less mass to the primary one with more mass. The latter may be explained by either the cyclic magnetic activity on the two components or the light-time effect due to a third body. With the absolute physical parameters, we investigated its evolutionary status, and find that LO And is an unevolved contact binary undergoing thermal relaxation oscillation, which will eventually coalesce into a single star with rapid rotation.

Key words: stars: binaries: close — stars: binaries: eclipsing — stars: individual (LO And)

1 INTRODUCTION

Eclipsing contact binaries are W UMa-type binaries which are composed of two dwarf stars embedded in a common convective envelop. Their spectral types span from F to K (Rucinski 1993). The orbital-period distribution peaks in the 8-12 hr range (Hilditch 2001). The light curves tend to have maxima, which are strongly curved, and minima, which are nearly equal in depth, so they are the EW-type light curves. From a morphological perspective, W UMa-type binaries can be classified into two subtypes: A subtype and W subtype (Binnendijk 1970). For a W-subtype system, the more massive component has a lower surface temperature than the less massive component; this reverses for the A-subtype system. In addition, W-subtype binaries tend to have larger mass ratio, shorter period and later spectral type than the A-subtype ones. Based on their radial-velocity curves, an A-subtype system shows that the middle of the decreasing branch of the primary star's radial-velocity curve occurs at phase zero, while the W-subtype system displays the opposite phenomenon, that is, the middle of the increasing branch of the primary star's radial-velocity curve occurs at phase zero (Binnendijk 1970). As suggested by Lucy (1976), the A-subtype systems are overcontact and have achieved thermal equilibrium as a result of nuclear evolution, with stable orbital periods and light curves, while the W-subtype systems tend to be in marginal contact and unstable, and they might be undergoing Thermal Relaxation Oscillation (TRO, Lucy 1976). These significant differences between the two subtypes imply that they followed distinct evolutionary pathways (Zhang et al. 2020). Thus, determination of the subtype of contact binaries could be helpful for understanding their formation and evolution.

Many W UMa-type binaries exhibit various period changes, such as continuous increase/decrease, cyclic oscillation or a combination of these variations. The secular period increase or decrease, in general, implies mass exchange/loss or magnetic braking. The cyclic variation could be an indicator of the cyclic magnetic activity or an underlying third body. In particular, Pribulla & Rucinski (2006) found that the incidence of

triple stars is not lower than $59\% \pm 8\%$. In fact, it is expected that all contact binaries should host at least one additional companion, because a triple system seems to be a necessary stage during the formation of contact binaries (Eggleton & Kiseleva-Eggleton 2001).

By relying on photographical observations, Weber (1963) first detected LO And, short for LO Andromeda (=TYC 3637-416-1, NSV 14569, NSVS 3561083, CSV 8853, WR 136), and classified it as a probable Cepheid variable. Diethelm & Gautschy (1980) made visual observations and deduced a preliminary ephemeris with a period of 0.190429 d. Meanwhile, they made photoelectric observations and reported the first photoelectric light curve, which was thought to cover a complete cycle. Boninsegna (1983) collected 102 light-minimum times and improved the ephemeris, such that the period provided by Diethelm & Gautschy (1980) was confirmed to be roughly half of the real value. They presented the first full light curve with the real period and found that LO And exhibits a typical EW-type luminosity variation. Gürol & Müyesseroğlu (2005) re-performed the photoelectric observations and derived the photometric solution of this system. They concluded that LO And is an A-subtype contact binary with a degree of contact of $f = 30.6\%$ and mass ratio $q = 0.371$. Nelson & Robb (2015) performed both photometric and spectroscopic observations. They found a significant magnitude difference between two maxima in their light curves, i.e., the O'Connell effect (O'Connell 1951). They applied a spot model to the light-curve fit and guessed that the spot was migrating because the light curves reported by Gürol & Müyesseroğlu (2005) did not manifest any significant asymmetry. In contrast to Gürol & Müyesseroğlu (2005), Nelson & Robb (2015) argued that LO And is a W-subtype contact binary. In addition to the uncertain photometric nature of LO And, its orbital period variation merits further investigation. Both Gürol & Müyesseroğlu (2005) and Nelson & Robb (2015) revealed that a secular increase and periodic variation in its orbital period exist. The former was attributed to mass transfer. However, the latter was subjectively assumed to originate from the Light Time Effect (LiTE, Irwin 1952) of the putative third star. There is also an alternative explanation, i.e., the magnetic activity cycle. At least, they did not have strong evidence to rule out magnetic activity. With the benefit of follow-up observations, a large number of new high-precision eclipse timings can be determined, which make the determination of the orbital period variations of LO And possible. To gain insight into the photometric nature of LO And and the possible origins of the orbital period variations, we conducted multi-band and high-precision photometric observations.

Table 1 Coordinates of Target Star, Comparison Star and Check Star

Object	Name	$\alpha(2000)$	$\delta(2000)$
Target	LO And	$23^{\rm h}27^{\rm m}06^{\rm s}.680$	$45^\circ33'22''.100$
Comparison	TYC3637–720–1	$23^{\rm h}27^{\rm m}19^{\rm s}.405$	$45^\circ28'01''.544$
Check	TYC3637–299–1	$23^{\rm h}26^{\rm m}26^{\rm s}.519$	$45^\circ30'37''.795$

2 PHOTOMETRIC OBSERVATIONS

We observed the W UMa-type binary, LO And, on two nights in September 2016 by using the 85-cm reflecting telescope at the Xinglong Station of National Astronomical Observatories, Chinese Academy of Sciences. During the observations, we adopted the standard *BVR* Johnson-Cousins filters and obtained a total of 2280 images, as well as 20 bias and 61 flat images. In the field of view of the target, we selected two stars, TYC 3637–720–1 and TYC 3637-299-1, as the comparison star and check star, respectively. Their coordinates are listed in Table 1. Utilizing the aperture photometry package of the `Image Reduction and Analysis Facility` (`IRAF`[1]) software library, we reduced all images to the photometric data, which are compiled in Table 2, where Δm is the magnitude difference between LO And and the comparison star. The phases were calculated referencing the period of 0.38043556 d determined by Nelson & Robb (2015). The corresponding light curves are plotted in the top panel of Figure 1. The typical EW-type luminosity variation for these light curves indicates an overcontact or at least near-contact geometrical configuration of LO And. In addition, through visual inspection, no significant asymmetry could be detected in these observed light curves. This implies either the absence of a spot or a symmetrical distribution of active spots.

3 SIMULTANEOUS SOLUTIONS OF LIGHT CURVES AND RADIAL-VELOCITY CURVES

With the latest version of the `Wilson-Devinney` (`W-D`) code (Wilson & Devinney 1971; Wilson 1979, 1990; Wilson & Van Hamme 2014), we simultaneously analyze the multi-band light curves and the radial-velocity curves by combining the radial-velocity data obtained by Nelson & Robb (2015) and our photometric data. As Wilson (1979) pointed out, the advantages of a simultaneous solution can effectively avoid inconsistencies among solutions of the separate curves and reduce the number of free parameters. According to the spectral

[1] IRAF is distributed by the National Optical Astronomy Observatory (NOAO) which is operated by the Association of the Universities for Research in Astronomy, Inc., under cooperative agreement with the National Science Foundation (NSF) (`http://iraf.noao.edu/`).

Table 2 *BVR* Band Photometric Data of LO And

B band			*V* band			*R* band		
JD (Hel.)	Phase	Δm	JD (Hel.)	Phase	Δm	JD (Hel.)	Phase	Δm
2457723.9303	0.583	–0.052	2457723.9306	0.584	–0.073	2457723.9307	0.584	–0.088
2457723.9310	0.585	–0.058	2457723.9313	0.586	–0.081	2457723.9314	0.586	–0.096
2457723.9329	0.590	–0.074	2457723.9331	0.591	–0.098	2457723.9333	0.591	–0.107
...	...	...	...	...	...	...	...	
2457725.0971	0.650	–0.226	2457725.0973	0.651	–0.229	2457725.0969	0.650	–0.246
2457725.0977	0.652	–0.222	2457725.0979	0.652	–0.227	2457725.0975	0.651	–0.257
2457725.0983	0.653	–0.228	2457725.0985	0.654	–0.240	2457725.0981	0.653	–0.258

The full data set of Table 2 is compiled as a supplementary file (ms2020–0337t2-mrt.txt) in machine-readable format. Here a portion is presented for guidance regarding its form and content.

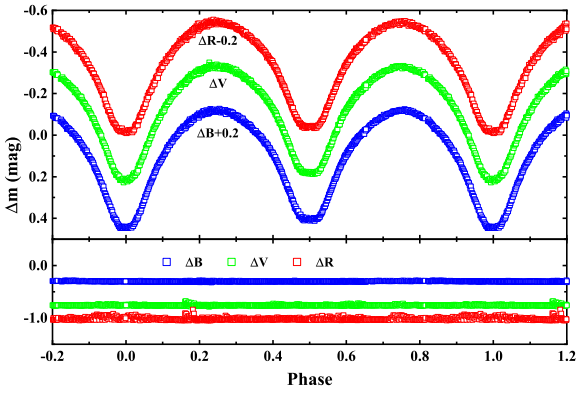

Fig. 1 *Top panel*: Photometric light curves in the *B*, *V* and *R* bands of LO And; *Bottom panel*: Corresponding magnitude differences between the comparison and check star.

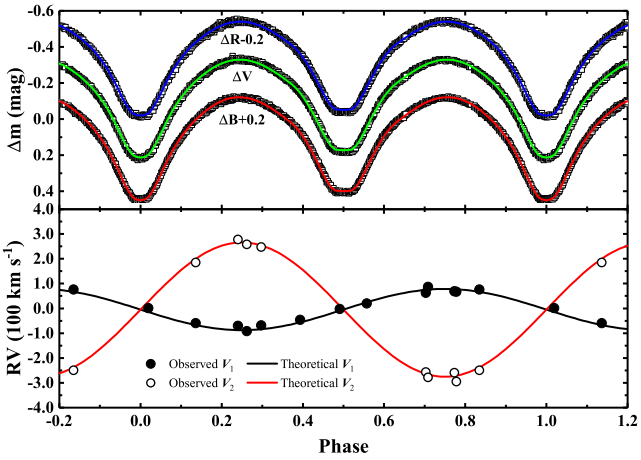

Fig. 2 *Top panel*: Observed (*hollow symbols*) and theoretical (*solid lines*) light curves of LO And; *Bottom panel*: Radial-velocity data and the fit curves.

type F5V derived by Nelson & Robb (2015), we estimated the surface temperature of the primary star to be $T_1 = 6650$ K by relying on the calibration of Cox (2000). By considering the convective envelope of the contact binary, we set the gravity-darkening exponents of two components of LO And to $g_1 = g_2 = 0.32$ (Lucy 1967), and bolometric albedos to $A_1 = A_2 = 0.5$ (Ruciński 1969). The square-root form is adopted for the nonlinear limb-darkening law and the bolometric and monochromatic coefficients are taken from Van Hamme (1993). Based on the above settings, the `W-D` code yields a convergent solution (see Table 3) after many iterations. With this solution, the theoretical light and velocity curves are then calculated and are plotted in Figure 2 as solid lines. The simultaneous solution suggests that the temperature of the secondary is somewhat lower than that of the primary, implying that LO And is an A-subtype contact binary. Because of the high precision and excellent symmetry in our multi-band light curves, the simultaneous solution should be more reliable than those of Nelson & Robb (2015) and Gürol & Müyesseroğlu (2005). In addition, we noted that in the study of Nelson & Robb (2015), LO And is classified as a W-subtype contact binary. But our simultaneous solution explicitly indicates that it belongs to the A-subtype. Perhaps, the light-curve asymmetry reported in the photometry of Nelson & Robb (2015) was due to the existence of a spot thus causing the spurious identification of the W subtype of LO And. In addition, the radial-velocity curves displayed in the bottom panel of Figure 2 indicate that the middle of the decreasing branch of the primary star's radial-velocity curve (the black solid line) occurs at phase zero. According to the theory of Binnendijk (1970), such systems will refer to an A-subtype system. Also, the high degree of contact, the low mass ratio and the spectral type of F5V satisfy the theoretical expectation (Lucy 1976) and the general statistical characteristics (Ruciński 1973, 1974) of A-subtype systems. The above facts suggest that the W UMa-type binary LO And should be an A-subtype system instead of a W-subtype one.

4 ORBITAL PERIOD CHANGES AND PHYSICAL ORIGINS

Both Gürol & Müyesseroğlu (2005) and Nelson & Robb (2015) have investigated the orbital period variations of

Table 3 Light- and Velocity-Curve Solutions of LO And

Parameters	Gürol & Müyesseroğlu (2005)	Nelson & Robb (2015)	This work
T_1 (K)	6500(fixed)	6650(fixed)	6650(fixed)
T_2 (K)	6465(±184)	6690(±24)	6621(±2)
$M_1(M_\odot)$	1.31(±0.18)	1.468(±0.048)	1.409(±0.04)
$M_2(M_\odot)$	0.49(±0.07)	0.447(±0.022)	0.449(±0.02)
$R_1(R_\odot)$	1.30(±0.05)	1.40(±0.01)	1.36(±0.01)
$R_2(R_\odot)$	0.85(±0.14)	0.84(±0.01)	0.83(±0.01)
$M_{\rm bol1}$ (mag)	3.67(±0.08)	3.45(±0.02)	3.47(±0.02)
$M_{\rm bol2}$ (mag)	4.62(±0.39)	4.53(±0.02)	4.56(±0.02)
$\log g_1$ (cgs)	4.32(±0.71)	4.32(±0.01)	4.32(±0.01)
$\log g_2$ (cgs)	4.26(±0.75)	4.24(±0.01)	4.25(±0.01)
$L_1(L_\odot)$	2.70(±0.08)	3.44(±0.06)	3.99(±0.05)
$L_2(L_\odot)$	1.13(±0.35)	1.27(±0.02)	1.43(±0.02)
q	0.371(±0.002)	0.305(±0.004)	0.319(±0.0004)
$\Omega_1 = \Omega_2$	2.548(±0.026)	2.401(±0.009)	2.443(±0.0009)
i (deg)	78.67(±0.62)	80.1(±0.6)	80.138(±0.055)
a (sol.rad.)	—	2.74(±0.02)	2.72(±0.03)
V_γ (km· s^{-1})	—	–3.0(±0.8)	–4.83(±0.8)
Spot co-latitude (deg)	—	97(±10)	—
Spot longitude (deg)	—	45(±5)	—
Spot radius (deg)	—	33(±2)	—
Spot temp factor	—	0.9765(±0.005)	—
$L_1/(L_1+L_2)(B)$	0.7175	—	0.73670(±0.00037)
$L_1/(L_1+L_2)(V)$	0.7061	0.7330(±0.0010)	0.73574(±0.00035)
$L_1/(L_1+L_2)(R)$	—	0.7339(±0.0009)	0.73512(±0.00038)
$L_1/(L_1+L_2)(I)$	—	0.7348(±0.0008)	—
r_1 (pole)	0.4524(±0.0058)	0.4706(±0.0003)	0.4656(±0.0001)
r_1 (side)	0.4873(±0.0081)	0.5103(±0.0005)	0.5037(±0.0002)
r_1 (back)	0.5189(±0.0115)	0.5414(±0.0008)	0.5338(±0.0002)
r_2 (pole)	0.2911(±0.0099)	0.2795(±0.0012)	0.2755(±0.0005)
r_2 (side)	0.3055(±0.0124)	0.2937(±0.0015)	0.2885(±0.0006)
r_2 (back)	0.3501(±0.0251)	0.3427(±0.0035)	0.3309(±0.0012)
$f = \frac{\Omega_{\rm in}-\Omega_1}{\Omega_{\rm out}-\Omega_{\rm in}}$	0.306	0.398(±0.062)	0.324(±0.009)

LO And. They concluded that the orbital period of this system is undergoing a continuous increase and a periodic oscillation, where the continuous period increase has been conclusively explained by mass transfer from the less massive secondary to the more massive primary, while periodic oscillation was contributed to the LiTE of the third body. In view of the recently accumulated high-precision eclipse timings, it is still necessary to reanalyze the orbital period variation. First, all eclipse timings of LO And reported in the literature and the $O-C$ gateway[2] are collected, where 318 data points are obtained. Second, we searched all available databases of various survey missions, and found that LO And was observed by the following five surveys: (1) Northern Sky Variability Survey (NSVS[3], Woźniak et al. 2004), (2) Wide Angle Search for Planets (WASP[4], Butters et al. 2010), (3) Brno Regional Network of Observers (BRNO[5], Hajek 2006; Zejda 2006), (4) All-Sky Automated Survey for SuperNovae (ASAS-SN[6], Shappee et al. 2014; Jayasinghe et al. 2019) and (5) Transiting Exoplanet Survey Satellite (TESS[7], Ricker et al. 2015). From the data archives of the above surveys, we extracted the photometric data of LO And and determined 332 eclipse timings, of which 121 are from WASP and 211 are from the TESS mission. Finally, together with two eclipse timings derived from our observations, a total of 652 data points were collected and compiled in Table 4.

For the sake of uniformity, we converted all these eclipse timings to the Barycentric Julian Date (BJD) form. Then, we calculated their $O-C$ values using the following linear ephemeris derived by Nelson & Robb (2015)

$$\mathrm{Min.I} = \mathrm{BJD}2445071.059639 + 0.38043556E. \quad (1)$$

As shown in the top panel of Figure 3, the $O-C$ values follow a clear upward parabolic trend, indicating that the orbital period is undergoing a long-term increase. In view of the errors in these data, we set the weight to one for the visual (vis) and photographic (pg) data, and eight for the photoelectric (PE) and charge-coupled device (CCD) data. Because the $O-C$ value of the eclipse timing BJD2457264.447303 obviously deviates from the general trend of the whole $O-C$ curve, it is not adopted in the following analysis. Based on the least-squares method, we

[2] http://var.astro.cz/ocgate/
[3] http://skydot.lanl.gov/nsvs/nsvs.php
[4] https://wasp.cerit-sc.cz/form
[5] http://var2.astro.cz/EN/brno/index.php
[6] https://asas-sn.osu.edu/variables
[7] https://heasarc.gsfc.nasa.gov/docs/tess/

Table 4 Calculated and Collected Eclipse Timings of LO And

HJD (2400000+)	BJD (2400000+)	Method	Error	Type	Ref.	HJD (2400000+)	BJD (2400000+)	Method	Error	Type	Ref.
36458.43700	36458.437403	pg	—	I	1	54361.56286	54361.563623	CCD	0.00047	II	52
37904.46000	37904.460385	pg	—	I	1	54362.51340	54362.514163	CCD	0.00042	I	52
38255.59200	38255.592384	pg	—	I	1	54363.46551	54363.466273	CCD	0.00052	II	52
...	...	...	...	...	...	...	...	...	...	...	...
54360.43214	54360.432903	CCD	0.00023	II	52	—	58787.427040	CCD	0.00008	I	82
54360.61230	54360.613063	CCD	0.00160	I	56	—	58787.617360	CCD	0.00009	II	82
54360.61317	54360.613933	CCD	0.00032	I	52	—	58787.807600	CCD	0.00007	I	82

The full data set of Table 4 is compiled as a supplementary file (ms2020–0337t4-mrt.txt) in machine-readable format. Here a portion is presented for guidance regarding its form and content.

References: 1. Berthold & Boninsegna (1985); 2. Diethelm & Gautschy (1980); 3. Boninsegna (1983); 4. Bob Nelson's $O-C$ files, 2013 (https://www.aavso.org/bob-nelsons-o-c-files); 5. http://var.astro.cz/ocgate/; 6. Rousselot (1984); 7. Isles (1986); 8. Diethelm et al. (1986); 9. Blättler et al. (1987); 10. Acerbi et al. (1989a); 11. Andrakakou et al. (1989); 12. Acerbi et al. (1989b); 13. Acerbi et al. (1990b); 14. Isles (1992); 15. Acerbi et al. (1990c); 16. Acerbi et al. (1990a); 17. Acerbi et al. (1990d); 18. Acerbi et al. (1991a); 19. Acerbi et al. (1991b); 20. Blättler et al. (1992); 21. Acerbi et al. (1992a); 22. Acerbi et al. (1992b); 23. Hübscher et al. (1993); 24. Hübscher et al. (1994); 25. Agerer & Hübscher (1995); 26. Blättler et al. (1996); 27. Acerbi et al. (1995); 28. Acerbi et al. (1997); 29. Agerer & Hübscher (1997); 30. Blättler et al. (1997); 31. Blšttler et al. (1998); 32. Juryšek et al. (2017); 33. Agerer & Hübscher (2001); 34. Nelson (2001); 35. Brát et al. (2007); 36. Safar (2003); 37. Agerer & Hübscher (2002); 38. Blaettler et al. (2001); 39. Baldinelli et al. (2002); 40. Dvorak (2003); 41. Nelson (2003); 42. Gürol & Müyesseroğlu (2005); 43. Kotkova & Wolf (2006); 44. Zejda (2004); 45. Nagai (2004); 46. Gürol et al. (2007); 47. Hübscher et al. (2005); 48. Hübscher et al. (2006); 49. Parimucha et al. (2007); 50. Doğru et al. (2007); 51. Hübscher & Walter (2007); 52. calculated times based on WASP data; 53. Hübscher et al. (2009); 54. Parimucha et al. (2009); 55. Nagai (2008); 56. Hübscher et al. (2008); 57. Dvorak (2008); 58. Hübscher et al. (2010); 59. Diethelm (2009); 60. Parimucha et al. (2011); 61. Demircan et al. (2011); 62. Nagai (2011); 63. Hübscher (2011); 64. Diethelm (2011); 65. Parimucha et al. (2013); 66. Nagai (2012); 67. Gürsoytrak et al. (2013); 68. Hoňková et al. (2013); 69. Nelson (2013); 70. Hoňková K. et al. (2014); 71. Nagai (2013); 72. Diethelm (2013); 73. Hübscher (2014); 74. Hoňková et al. (2015); 75. Hübscher (2015); 76. Parimucha et al. (2016); 77. Hübscher (2017); 78. Nagai (2016); 79. Bahar et al. (2017); 80. This paper; 81. http://var2.astro.cz/brno/; 82. calculated times based on TESS data.

derived a quadratic ephemeris

$$\begin{aligned}\mathrm{Min.I} = \mathrm{BJD}2445071.06516 + 0.38043550E \\ + 1.127\times10^{-10}E^2.\end{aligned} \quad (2)$$

The quadratic term reveals an orbital-period increase at a rate of $\dot{P} = 2.16\times10^{-7}\,\mathrm{d\,yr^{-1}}$, implying a continuous mass transfer from the less massive secondary to the more massive primary. With the formula (Pringle 1975)

$$\dot{M}_2 = -\dot{M}_1 = -\frac{\dot{P}}{3P}\frac{M_1M_2}{(M_1-M_2)}, \quad (3)$$

and the absolute physical parameters, we derived the mass transfer rate as $\dot{M}_2 = -\dot{M}_1 = -1.25\times10^{-7}M_\odot\,\mathrm{yr^{-1}}$. Thus, we may estimate the mass transfer timescale of the secondary $\tau_{\rm mt} = \frac{M_2}{\dot{M}_2} = 3.592\times10^6$ yr. However, its thermal timescale is $\tau_{\rm th} \sim \frac{GM_2^2}{R_2L_2} \sim 5.310\times10^6$ yr (Paczyński 1971). Clearly, the mass-transfer timescale of the secondary is significantly shorter than its thermal timescale, implying that the mass transfer in this binary is thermally unstable. Therefore, LO And cannot achieve thermal equilibrium, and might be evolving from a contact configuration to a marginal contact or even semi-detached status predicted by TRO theory (Lucy 1976; Flannery 1976; Li et al. 2004, 2005, 2008).

After subtracting the parabola, a cyclic oscillation can be visually identified (see the $(O-C)_2$ curve in the middle panel of Fig. 3). Usually, there are two alternative explanations for the cyclic oscillation: the periodic magnetic activity on one or both components of the binary and the LiTE due to a third body. We shall examine each case.

4.1 Cyclic Period Change and Its Possible Origin of Cyclic Magnetic Activity

When considering the cause of cyclic magnetic activity, we performed a least-squares sinusoidal fit to the $(O-C)_2$ residuals and derived the equation

$$\begin{aligned}(O-C)_2 = -0.0016(\pm0.0013) - 0.0075(\pm0.0016) \\ \times\sin[0.00022(\pm0.00002)E - 0.9548(\pm0.368)].\end{aligned} \quad (4)$$

Equation (4) is plotted in the middle panel of Figure 3(a) with a blue solid line. The comprehensive fitting curve that includes the quadratic and sinusoidal function is plotted in the top panel of Figure 3(a), and the final residuals are presented in the bottom panel. The sinusoidal fit reveals a cyclic period change with an amplitude of 0.0075 d (=648 s) and a period of 29.24 yr. First, this cyclic variation for $(O-C)_2$ values should not result from the phase shift of the real eclipse timings yielded by a migratory spot, because the amplitude of 0.0075 d (=648 s) is far larger than the typical value of $\sim$ 300 s yielded by the migratory spot (Tran et al. 2013). If the $(O-C)_2$ variation is rooted in cyclic magnetic activity, Applegate's theoretical model (Applegate 1992; Lanza et al. 1998; Lanza & Rodonó 2002) should be carefully checked. According to this model, the active component of a binary system is divided into an inner kernel and outer shell. The strong magnetic activity of the active component could cause differential rotation between the kernel and shell. This will yield a continuous change in the quadrupole moment and the angular momentum of the system, sequentially resulting

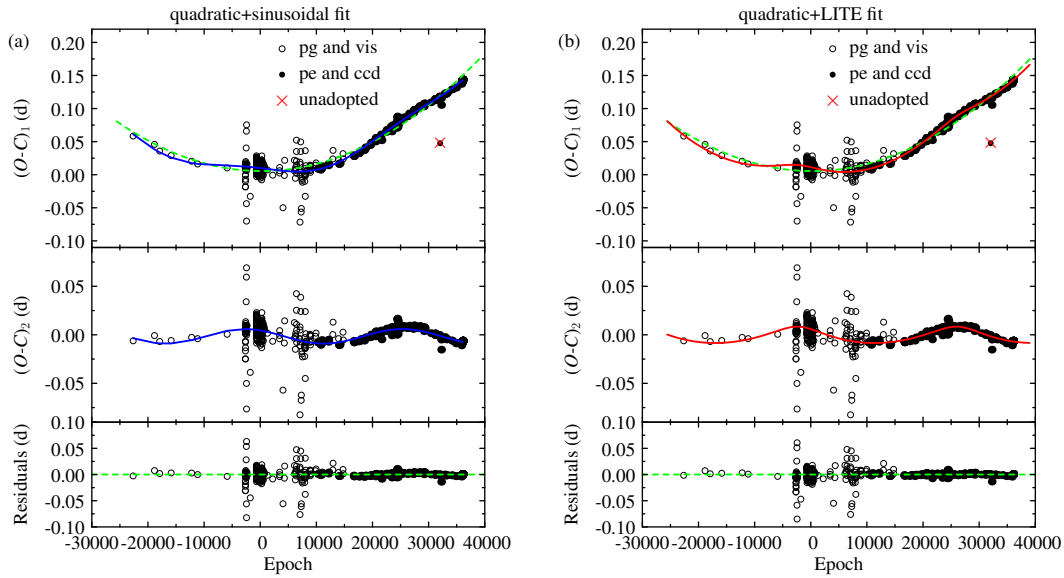

Fig. 3 $(O-C)$ diagram and residuals of LO And. *Top panels*: $(O-C)_1$ curve calculated with the linear ephemeris of Eq. (1). The *blue solid line* in Fig. 3(a) signifies the fitting curve combining the quadratic ephemeris with sinusoidal function, while the *red solid line* in Fig. 3(b) is the fitting curve combining the quadratic with LiTE, and the *dashed line* refers to the parabolic part. *Middle panels*: $(O-C)_2$ diagram after removing the parabolic part. The *blue solid line* in Fig. 3(a) corresponds to the fitting curve of the sinusoidal function, and the *red solid line* in Fig. 3(b) represents the fitting curve utilizing the function `LiTE3` of the Python package `OCFit`. *Bottom panels*: Final residuals.

in the changes to the components' oblateness and radial differential rotation. Finally, the orbital period of the binary system is constantly modulated via gravitational coupling. Considering the modulation period ($P_{\rm mod} = 29.24$ yr), the amplitude ($A = 0.0075$ d) obtained above, and the absolute physical parameters derived in the previous section, we calculated the parameters of Applegate's model. These parameters are the amplitude of orbital period modulation ΔP, the variation of quadruple moment ΔQ, the angular momentum transfer ΔJ, the variation of angular velocity $\Delta\Omega/\Omega$, the required energy ΔE, the luminosity variation $\Delta L/L$ and the magnetic field B, which are listed in Table 5. The magnetic-activity parameters for both the primary and secondary of LO And seem to follow the typical values required by Applegate's model, implying the observed period changes could be due to the cyclic magnetic activity of either of the two components. Because the energy is transferred from the primary to the secondary in this contact binary system, the temperature gradient in the surface of the primary should be increased, so that its convection envelope should be increased. As a result, the magnetic activity in the primary becomes relatively strong. In addition, the photometric study of Nelson & Robb (2015) also suggested that there may be an active starspot on the surface of the primary component of LO And. Thus, if the periodic variation in the orbital period of LO And indeed originates from the magnetic activity, it should be more likely that the cyclic period variation is caused by the magnetic activity of its primary, just like AR Boo (Han et al. 2019). However, the photometric observations made by us and Gürol & Müyesseroğlu (2005) did not reveal any asymmetry in its light curves, indicating the absence of magnetic activity. Perhaps, the asymmetries of these light curves were just masked by the symmetrical distribution of the active spots and the scatter in the data.

To resolve this issue more firmly, we analyzed all available light curves of LO And obtained from the literature and from surveys (see Fig. 4). If the periodic oscillation in its orbital period is indeed caused by cyclic magnetic activity, there should be some additional observable effects in its light curves, such as periodic variations of the O'Connell effect (O'Connell 1951), maximum luminosity and color of systems. These effects will form crucial evidence for judging the magnetic activity interpretation of the periodic period variation (Kalimeris et al. 1994; Kim et al. 1997). Because most survey missions have performed photometric observations in either a single-color or wide-band filter, it is almost impossible to trace long periodic variations in maximum luminosity or color. The O'Connell-effect variation could be a plausible indicator for the cyclic magnetic activity (Hu et al. 2020; Pi et al. 2019, 2014). Based on the collected light curves of LO And, we calculated two kinds of measurements for the O'Connell effect, i.e., the magnitude differences (Δm) between two maxima and

Table 5 Parameters of Applegate's Model for Generating the Observed Cyclic Period Variation of LO And

Parameter	Primary		Secondary	Typical Value	Unit
$P_{\rm mod}$		29.24($\pm$0.21)		—	yr
ΔP		1.68($\pm$0.13)$\times10^{-6}$		10^{-5}–10^{-6}	d
$\Delta P/P$		4.41($\pm$0.33)$\times10^{-6}$		10^{-5}–10^{-6}	—
ΔQ	4.93($\pm$0.37)$\times10^{49}$		1.57($\pm$0.12)$\times10^{49}$	10^{49}	g cm^2
ΔJ	1.70($\pm$0.13)$\times10^{47}$		0.76($\pm$0.06)$\times10^{47}$	10^{46}–10^{47}	g cm^2 s^{-1}
$\Delta\Omega/\Omega$	3.55($\pm$0.27)$\times10^{-4}$		1.34($\pm$0.10)$\times10^{-3}$	0.01	—
ΔE	3.47($\pm$0.11)$\times10^{40}$		5.83($\pm$0.33)$\times10^{40}$	—	erg
$\Delta L/L$	0.009($\pm$0.001)		0.043($\pm$0.002)	< 0.1	—
B	2025($\pm$233)		2838($\pm$256)	10^3–10^4	G

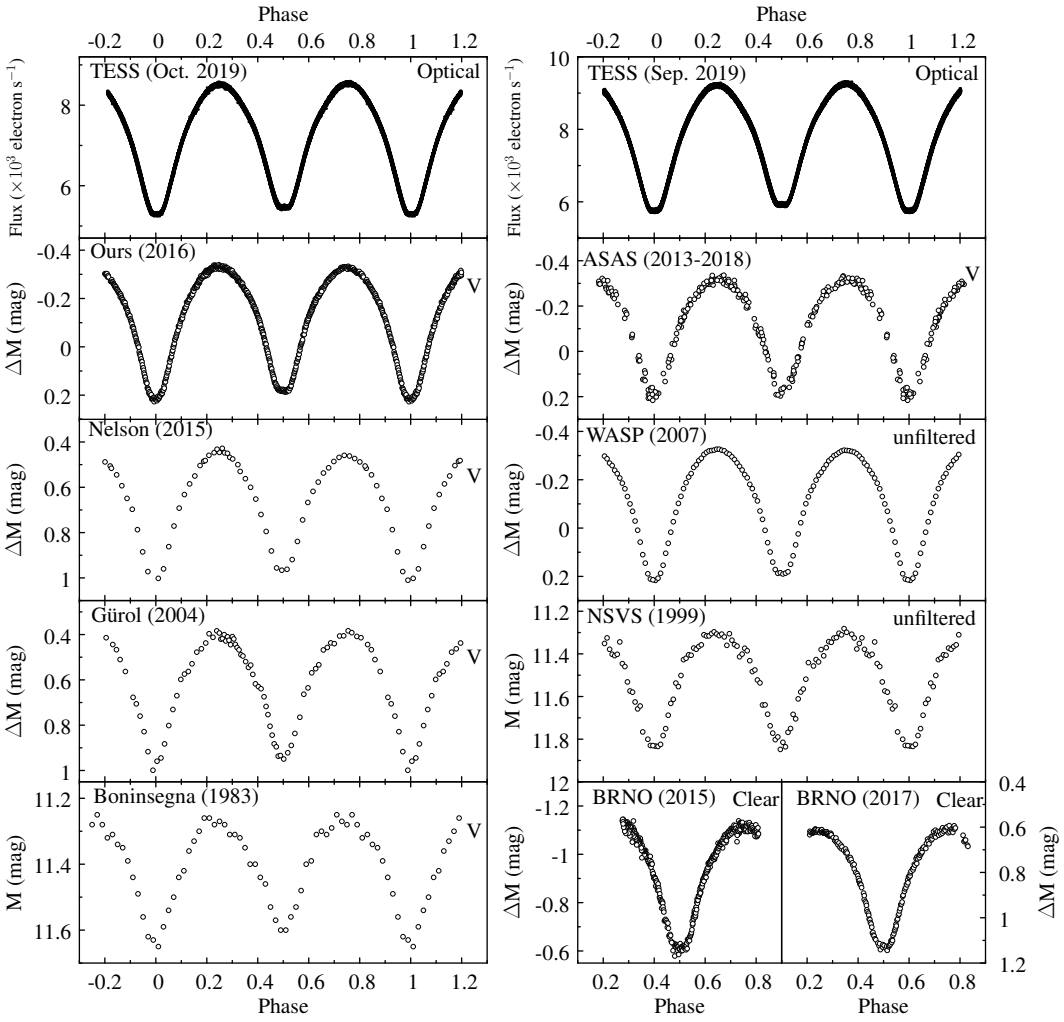

Fig. 4 Light curves obtained from literatures, survey missions and our observations.

the O'Connell Effect Ratio (OER, McCartney 1997). By fitting the light curves around the maxima, the magnitudes for the maxima are estimated and the magnitude difference is then calculated with equation

$$\Delta m = m_{\rm Max.II} - m_{\rm Max.I}\,. \tag{5}$$

The OER is the ratio of the areas beneath two maxima of a phased light curve. By partitioning a phased light curve into n equally wide bins, OER is then calculated with its definition (McCartney 1997)

$$\mathrm{OER} = \frac{\Sigma_{k=1}^{n/2}(I_k - I_1)}{\Sigma_{k=(n/2)+1}^{n}(I_k - I_1)}\,, \tag{6}$$

where I_1 is the average magnitude/flux in the primary-minimum bin and I_k is the average magnitude/flux in the kth bin. By considering the different number of data points in each light curve, in our calculations, all light curves were divided into 40 bins. In addition, because the

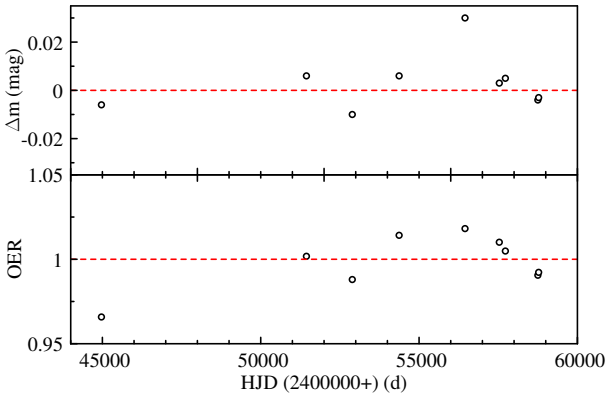

Fig. 5 Δm and OER as a function of HJD.

O'Connell effect has a weak correlation with wavelengths (Davidge & Milone 1984), we should use a uniform band to examine the possible changes in the O'Connell effect. But, for some surveys, such as NSVS and WASP, no filter (NSVS and WASP before 2006) or broadband filter (400 nm $\sim$ 700 nm bandpass) (WASP after 2006) was adopted for their observations. Therefore, we measure the O'Connell effect based on the different bandpass light curves. In addition, if multi-color light curves are available, we will choose light curves in the V band to reduce the possible impacts from the different filters. The reasons are twofold: (1) the V-band light curve is the one most commonly found in these observations of LO And, and (2) the wavelength corresponding to the V band is the most sensitive one for CCD observations and is close to the middle wavelength of the optical bandpass. The Δm and OER for those light curves are listed in the last two columns of Table 6 and plotted as a function of Heliocentric Julian Date (HJD) in Figure 5. According to Applegate's theory, the O'Connell effect should change periodically. However, any significant periodicity cannot be identified from both Δm and OER. On the contrary, the amplitudes of their variations are so small and seem more like irregular fluctuations due to the uncertainty of observations. Of course, because those light curves obtained from the surveys are phased using the data that cover at least one observing season, this treatment may reduce the amplitudes of the O'Connell-effect variation. In addition, if the active spots are distributed symmetrically, the light curves would be symmetrical. These possible factors could puzzle us when trying to detect the underlying periodicity of the O'Connell-effect variation.

4.2 Cyclic Period Change and Its Third-Body Interpretation

When considering a third body orbiting LO And as the cause of its $(O-C)_2$ variation, we should adopt the general light-time ephemeris (Irwin 1952) to fit the $(O-C)_2$ variation. The theoretical formula for the LiTE of the third body has been derived by Irwin (1952) as

$$\tau_{\rm LiTE} = \frac{a_{12}\sin(i_3)}{c}\Big[\frac{1-e_3^2}{1+e_3\cos(\nu_3)}\sin(\nu_3+\omega_3) + e_3\sin(\omega_3)\Big], \quad (7)$$

where $a_{12}\sin(i_3)$ and i_3 signify the semi-major axis and orbital inclination of the third-body respectively, e_3 is its eccentricity, c is the speed of light, and ν_3 and ω_3 represent the true anomaly of the binary orbit around the system's barycenter and the longitude of pericenter, respectively. In addition, the orbital period of the third body P_3 and the time of pericenter passage t_{03} are inherently related to the calculation of the true anomaly ν_3, which can be solved with the Kepler equation. Although the orbital inclination of the third body i_3 could not be derived from only the $(O-C)_2$ fit, the projected semi-major axis $a_{12}\sin(i_3)$ can be calculated from the semi-amplitude K_3 of the $(O-C)_2$ variation according to the formula

$$K_3 = \frac{a_{12}\sin(i_3)\sqrt{1-e_3^2\cos(\omega_3)}}{c}, \quad (8)$$

and the mass function

$$f(M_3) = \frac{(M_3\sin i_3)^3}{(M_1+M_2+M_3)^2} = \frac{(a_{12}\sin i_3)^3}{P_3^2} \quad (9)$$

can then be determined.

In order to derive the orbital parameters of the assumed third body, we employed the `LiTE` package of the `OCFit` code (Gajdoš & Parimucha 2019) to fit the $(O-C)_2$ values. This package first determines initial values of the fitting parameters applying genetic algorithms to avoid deviations of the speculative initial parameters. These initial parameters are then input to Markov Chain Monte Carlo simulations. After sufficient iteration steps, the fitting parameters are finally determined. By combining these fitting parameters with Equations (8) and (9), both orbital and physical parameters of the third body around LO And are calculated and summarized in Table 7. Among them, the mass M_3 and orbital semi-major axis a_3 of the third body are determined based on the coplanar-orbit assumption, i.e., $i_3 = i = 80.138°$. The fitting curve of the $(O-C)_2$ values is plotted in the middle panel of Figure 3(b). Taken together with the quadratic fit, the comprehensive result is shown in the top panel of Figure 3(b), and the final residuals are presented in the bottom panel of Figure 3(b) where no significant change can be found. When comparing these parameters with the results of Gürol & Müyesseroğlu (2005) and Nelson & Robb (2015), we find that our fit reveals that the third body of LO And has a higher orbital eccentricity and more mass. The high orbital eccentricity means

Table 6 Long-term O'Connell Effect Variations

Observation	Year	Mean HJD[a]	Band	Δm (mag)	OER
TESS	2019	58776	Optical	-0.003[b]	0.99226
TESS	2019	58751	Optical	-0.004[b]	0.99055
Ours	2016	57725	*V*	0.005	1.00488
ASAS	2013-2018	57533	*V*	0.003	1.01009
Nelson & Robb	2013	56451	*V*	0.03	1.01816
WASP	2007	54370	400-700 nm	0.006	1.01419
Gürol & Müyesseroğlu	2003	52891	*V*	-0.01	0.98800
NSVS	1999	51443	unfiltered	0.006	1.00177
Boninsegna	1981-1983	44970	*V*	-0.006	0.96583

[a] The average value of HJD of the observational data points for the corresponding light curve. [b] Because the TESS light curves were depicted in the form of flux, their Δm were calculated with equation $m_2 - m_1 = -2.5\log\frac{F_2}{F_1}$.

that the LiTE of the third body is more reasonable when explaining the cyclic variation of the $(O-C)_2$ values than the cyclic magnetic activity. In view of the existence of the third body, we also tried to adjust the parameters of the third light in the `W-D` code. However, any significant third light was not found in the light curve for each band, which is the same as the photometric solutions obtained by both Gürol & Müyesseroğlu (2005) and Nelson & Robb (2015). If there indeed exists a third body orbiting the binary LO And, it may be a very cool component since it does not contribute any significant luminosity to the system. Of course, it is very difficult, even unreal, to detect the third light from the light curve of a contact binary system. The most direct evidence for the existence of the third body is the transiting circumbinary event or the variation in the binary system's γ-velocity (V_γ). Nevertheless, additional eclipses, in general, are extremely rare or detected with great difficulty, because both the occurrence of transiting circumbinary events and observation methods need quite strict requirements (Klagyivik et al. 2017). The identification of the γ-velocity variation needs at least two sets of radial-velocity curves obtained at different times. With the equation

$$\Delta V_\gamma = \frac{G^{\frac{1}{2}}}{K_3^{\frac{1}{2}} c^{\frac{1}{2}}} \frac{M_3^{\frac{3}{2}}}{M_1 + M_2 + M_3}, \tag{10}$$

we estimated the amplitude of γ-velocity variation to be $\Delta V_\gamma = 1.52\ \mathrm{km\,s^{-1}}$ for LO And. For this paper, $V_\gamma = -4.83\ \mathrm{km\,s^{-1}}$ was derived from the radial-velocity curves obtained from spectroscopic observations between 2007 and 2013. In order to confirm the γ-velocity variation, we should perform another set of spectroscopic observations in about 2025 to obtain another γ-velocity with the largest difference from the current one.

5 DISCUSSIONS AND CONCLUSIONS

In this paper, the simultaneous solutions of the multi-color light curves and the radial-velocity curves suggest that LO And is an A-subtype overcontact binary, instead of the W-subtype inferred by the earlier work (Nelson & Robb 2015). Also, the absolute elements are further improved. The orbital period of LO And shows a long-term increase and a periodic oscillation. The long-term period increase is due to the mass transfer from the secondary to the primary. For the periodic oscillation, we discuss two possible physical origins: cyclic magnetic activity and LiTE of the third body. Although any significant cyclic variation cannot be detected in the O'Connell effects from the light curves covering about 28 yr, the possibility that the periodic variation in the orbital period of LO And is caused by magnetic activity still cannot be ruled out. Thus, additional evidence of cyclic magnetic activity or a third body, such as the cyclic effect in characteristic emission/absorption lines due to activity spots, the cyclic variation of γ-velocity or the third-body spectrum in high-resolution spectroscopy, should be further studied to resolve this issue more firmly.

With the computed absolute elements, we can estimate the current evolutionary status of LO And using the $\log T - \log L$ (i.e., Hertzsprung-Russell) diagram. Figure 6 shows the locations of two components of LO And, together with some other A-subtype and W-subtype contact binaries. As can be seen in Figure 6, two components of LO And seem to be in good alignment with those of the A-subtype contact binary systems. In addition, the primary component is located between the Zero Age Main Sequence (ZAMS) and Terminal Age Main Sequence (TAMS) lines, indicating that it should not be an evolved star. The secondary component is located significantly below the ZAMS line, meaning that it is not yet evolved. However, it is quite difficult to infer its evolutionary status because the evolution of the secondary is dramatically affected by its contact with the primary. Perhaps, this significant deviation from the ZAMS line may be caused by the rapid expansion of the secondary owing to full energy transfer from the primary to the secondary, which dissipates a large amount of its thermal energy. In fact,

Table 7 Fitted Parameters for the LiTE of the Third Body Orbiting the Binary LO And

Parameter	Gürol & Müyesseroğlu (2005)	Nelson & Robb (2015)	This work	Unit
P_3	37.08	29.6	29.52(± 0.95)	yr
$a_{12}\sin(i_3)$	1.435	1.31	1.462(± 0.056)	au
e_3	0.275	0.262	0.354(± 0.029)	—
t_{03}	—	—	2444432(± 244)	d
ω_3	198	80.4	98.4(± 8.4)	deg
K_3	—	—	729(± 29)	s
$f(M_3)$	0.002150	0.00256	0.0036(± 0.0005)	$M_\odot$
M_3	0.21	0.22	0.256(± 0.018)	$M_\odot$
a_3	—	—	10.8(± 0.006)	au

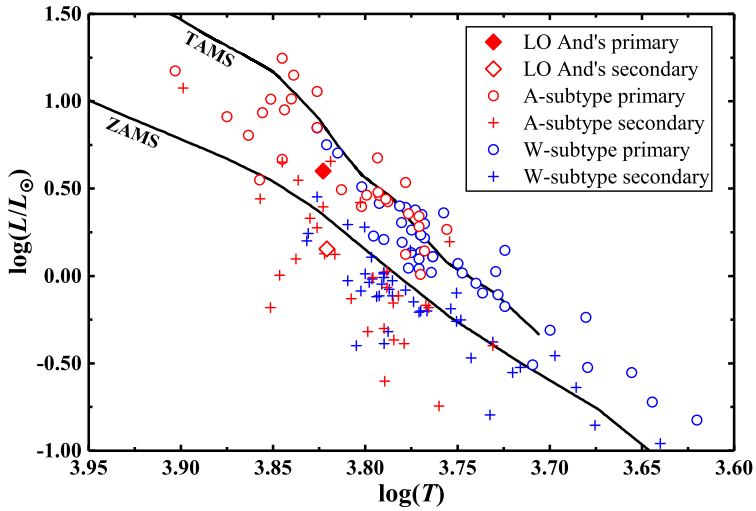

Fig. 6 Locations of two components of LO And in the $\log T - \log L$ diagram. The *solid lines* represent the ZAMS and TAMS obtained from Girardi et al. (2000) for the solar chemical composition. The samples of A-subtype and W-subtype contact binaries were taken from Yakut & Eggleton (2005).

it is also consistent with unstable mass transfer from the secondary to the primary mentioned above. Anyway, LO And should be classified as an unevolved contact binary, and thus be undergoing TRO. Perhaps, after about a few dozen TROs, it could gradually evolve into the overcontact stage with an extremely low mass ratio. Finally, just like some low-mass-ratio and deep-contact binaries with secular period increase, such as V410 Aur, XY Boo (Yang et al. 2005), V857 Her (Qian et al. 2005), AH Cnc (Qian et al. 2006), QX And (Qian et al. 2007), EM Psc (Qian et al. 2008), V345 Gem (Yang et al. 2009), V1191 Cyg (Zhu et al. 2011), CK Boo (Yang et al. 2012), and DZ Psc (Yang et al. 2013), LO And will encounter the so-called Darwin instability and coalesce into a rapidly rotating single star (Hut 1980).

Acknowledgements We appreciate the support of the Joint Research Funds in Astronomy (Grant Nos. U1931115, U2031114, and U1731110) under cooperative agreement between the National Natural Science Foundation of China and the Chinese Academy of Sciences, and the staff of the Xinglong 85cm telescope. This work was partially supported by the Open Project Program of the Key Laboratory of Optical Astronomy, National Astronomical Observatories, Chinese Academy of Sciences.

We thank the following surveys for their valuable data: (1) NSVS (Woźniak et al. 2004), who collected data with the first generation Robotic Optical Transient Search Experiment; (2) WASP whose data (Butters et al. 2010) were provided by the WASP consortium, and the computing and storage facilities at the CERIT Scientific Cloud, reg. no. CZ.1.05/3.2.00/08.0144 which is operated by Masaryk University, Czech Republic; (3) ASAS (Shappee et al. 2014; Kochanek et al. 2017; Jayasinghe et al. 2019); (4) BRNO (Hajek 2006; Zejda 2006), a project administered by the Variable Star and Exoplanet Section of Czech Astronomical Society; (5) TESS (Ricker et al. 2015), where the photometric data were extracted from the MAST data archive at the Space Telescope Science Institute (STScI). The TESS mission is funded by the NASA Explorer Program.

References

Acerbi, F., Blättler, E., Boistel, G., et al. 1992a, BBSAG, 101

Acerbi, F., Crumrine, R. E., Diethelm, R., et al. 1990a, BBSAG, 95
Acerbi, F., Blättler, E., Boistel, G., et al. 1989a, BBSAG, 90
Acerbi, F., Benz, A., Blanchart, C., et al. 1989b, BBSAG, 92
Acerbi, F., Blanchart, C., Barani, C., et al. 1990b, BBSAG, 93
Acerbi, F., Blättler, E., Boistel, G., et al. 1990c, BBSAG, 94
Acerbi, F., Boistel, G., Boninsegnia, R., et al. 1990d, BBSAG, 96
Acerbi, F., Barani, C., Blättler, E., et al. 1991a, BBSAG, 97
Acerbi, F., Barani, C., Blättler, E., et al. 1991b, BBSAG, 98
Acerbi, F., Blättler, E., Boistel, G., et al. 1992b, BBSAG, 102
Acerbi, F., Bigi, M., Blättler, E., et al. 1995, BBSAG, 110
Acerbi, F., Blättler, E., Dalmazio, D., et al. 1997, BBSAG, 114
Agerer, F., & Hübscher, J. 1995, IBVS, 4222
Agerer, F., & Hübscher, J. 1997, IBVS, 4472
Agerer, F., & Hübscher, J. 2001, IBVS, 5016
Agerer, F., & Hübscher, J. 2002, IBVS, 5296
Andrakakou, M., Blättler, E., Busquets, J., et al. 1989, BBSAG, 91
Applegate, J. H. 1992, ApJ, 385, 621
Bahar, E., Yörükoğlu, O., Esmer, E. M., et al. 2017, IBVS, 6209
Baldinelli, L., Blaettler, E., Diethelm, R., et al. 2002, BBSAG, 127
Berthold, T., & Boninsegna, R. 1985, Mitt.Hartha Heft, 19
Binnendijk, L. 1970, VA, 12, 217
Blaettler, E., Diethelm, R., Guilbault, P., et al. 2001, BBSAG, 126
Blättler, E., Dalmazio, D., Dedoch, A., et al. 1996, BBSAG, 113
Blättler, E., Germann, R., Hainaut, V., et al. 1987, BBSAG, 82
Blättler, E., Boninsegna, R., Diethelm, R., et al. 1992, BBSAG, 99
Blättler, E., Dalmazio, D., Dedoch, A., et al. 1997, BBSAG, 115
Blšttler, E., Dedoch, A., Diethelm, R., et al. 1998, BBSAG, 116
Boninsegna, R. 1983, GEOS, EB 11
Brát, L., Zejda, M., & Svoboda, P. 2007, OEJV, 74
Butters, O. W., West, R. G., Anderson, D. R., et al. 2010, A&A, 520, L10, 1
Cox, A. N. 2000, Allen's Astrophysical Quantities (4th ed.; New York: Springer)
Davidge, T. J., & Milone, E. F. 1984, ApJS, 55, 571
Demircan, Y., Gürol, B., Gökay, G., et al. 2011, IBVS, 5965
Diethelm, R. 2009, IBVS, 5871
Diethelm, R. 2011, IBVS, 5960
Diethelm, R. 2013, IBVS, 6042
Diethelm, R., & Gautschy, A. 1980, IBVS, 1767
Diethelm, R., P.Elias, D., Germann, R., et al. 1986, BBSAG, 80
Doğru, S. S., Dönmez, A., Tüysüz, M., et al. 2007, IBVS, 5746
Dvorak, S. 2003, IBVS, 5378
Dvorak, S. 2008, IBVS, 5814
Eggleton, P., & Kiseleva-Eggleton, L. 2001, ApJ, 562, 1012
Flannery, B. P. 1976, ApJ, 205, 217
Gajdoš, P., & Parimucha, Š. 2019, OEJV, 197, 71
Girardi, L., Bressan, A., Bertelli, G., & Chiosi, C. 2000, Astron. Astrophys. Suppl. Ser., 141, 371
Gürol, B., & Müyesseroğlu, Z. 2005, AN, 326, 43
Gürol, B., Derman, E., Müyesseroğlu Z., et al. 2007, IBVS, 5791
Gürsoytrak, H., Demircan, Y., Gökay, G., et al. 2013, IBVS, 6075
Hajek, P. 2006, JAVSO, 35, 222
Han, Q. W., Li, L. F., Kong, X. Y., Li, J. S., & Jiang, D. K. 2019, New Astronomy, 66, 14
Hilditch, R. W. 2001, An Introduction to Close Binary Stars (Cambridge: Cambridge University Press)
Hoňková, K., Juryšek, J., Lehký, M., et al. 2015, OEJV, 0168
Hoňková, K., Juryšek, J., Lehký, M., et al. 2013, OEJV, 0160
Hoňková K., Juryšek, J., Lehký, M., et al. 2014, OEJV, 0165
Hu, K., Yu, Y. X., Zhang, J. F., & Xiang, F. Y. 2020, AJ, 160, 62
Hübscher, J. 2011, IBVS, 5984
Hübscher, J. 2014, IBVS, 6118
Hübscher, J. 2015, IBVS, 6152
Hübscher, J. 2017, IBVS, 6196
Hübscher, J., Agerer, F., Frank, P., & Wunder, E. 1994, BAV Mitt, 68
Hübscher, J., Agerer, F., & Wunder, E. 1993, BAV Mitt, 62
Hübscher, J., Lehmann, P. B., Monninger, G., Steinbach, H. M., & Walter, F. 2010, IBVS, 5918
Hübscher, J., Paschke, A., & Walter, F. 2005, IBVS, 5657
Hübscher, J., Paschke, A., & Walter, F. 2006, IBVS, 5731
Hübscher, J., Steinbach, H. M., & Walter, F. 2008, IBVS, 5830
Hübscher, J., Steinbach, H. M., & Walter, F. 2009, IBVS, 5874
Hübscher, J., & Walter, F. 2007, IBVS, 5761
Hut, P. 1980, A&A, 92, 167
Irwin, J. B. 1952, ApJ, 116, 211
Isles, J. 1986, BAA VSS Circ, 63
Isles, J. 1992, BAA VSS Circ, 73
Jayasinghe, T., Stanek, K. Z., Kochanek, C. S., et al. 2019, MNRAS, 485, 961
Juryšek, J., K., H., L., Š., et al. 2017, OEJV, 0179
Kalimeris, A., Rovithis-Livaniou, H., Rovithis, P., et al. 1994, A&A, 291, 765
Kim, C. H., Jeong, J. H., Demircan, O., Muyesseroglu, Z., & Budding, E. 1997, AJ, 114, 2753
Klagyivik, P., Deeg, H. J., Cabrera, J., Csizmadia, S., & Almenara, J. M. 2017, A&A, 602, A117
Kochanek, C. S., Shappee, B. J., Stanek, K. Z., et al. 2017, PASP, 129
Kotkova, L., & Wolf, M. 2006, IBVS, 5676
Lanza, A. F., & Rodonó, M. 2002, AN, 323, 424
Lanza, A. F., Rodonó, M., & Rosner, R. 1998, MNRAS, 296, 893
Li, L. F., Han, Z. W., & Zhang, F. H. 2004, MNRAS, 351, 137
Li, L. F., Han, Z. W., & Zhang, F. H. 2005, MNRAS, 360, 272
Li, L. F., Zhang, F. H., Han, Z. W., Jiang, D. K., & Jiang, T. Y. 2008, MNRAS, 387, 97
Lucy, L. B. 1967, ZA, 65, 89
Lucy, L. B. 1976, ApJ, 205, 208
McCartney, S. A. 1997, ASP Conf. Ser., 130, 129
Nagai, K. 2004, VSB, 42
Nagai, K. 2008, VSOLJ, 46
Nagai, K. 2011, VSOLJ, 51
Nagai, K. 2012, VSOLJ, 53
Nagai, K. 2013, VSOLJ, 55

Nagai, K. 2016, VSOLJ, 61
Nelson, R. H. 2001, IBVS, 5040
Nelson, R. H. 2003, IBVS, 5371
Nelson, R. H. 2013, IBVS, 6050
Nelson, R. H., & Robb, R. M. 2015, IBVS, 6134
O'Connell, D. J. K. 1951, PRCO, 2, 85
Paczyński, B. 1971, ARA&A, 9, 183
Parimucha, Š., Dubovský, P., Balud'ansky, D., et al. 2009, IBVS, 5898
Parimucha, Š., Dubovský, P., Kudak, V., & Perig, V. 2016, IBVS, 6167
Parimucha, Š., Dubovský, P., & Vaňko, M. 2013, IBVS, 6044
Parimucha, Š., Dubovský, P., Vaňko, M., et al. 2011, IBVS, 5980
Parimucha, Š., Vaňko, M., Pribulla, T., et al. 2007, IBVS, 5777
Pi, Q. F., Zhang, L. Y., Bi, S. L., et al. 2019, ApJ, 877, 75
Pi, Q. F., Zhang, L. Y., Li, Z. M., & Zhang, X. L. 2014, AJ, 147, 50
Pribulla, T., & Rucinski, S. M. 2006, AJ, 131, 2986
Pringle, F. E. 1975, MNRAS, 170, 633
Qian, S. B., He, J. J., Soonthornthum, B., et al. 2008, AJ, 136, 1940
Qian, S. B., Liu, L., Soonthornthum, B., Zhu, L. Y., & He, J. J. 2006, AJ, 131, 3028
Qian, S. B., Liu, L., Soonthornthum, B., Zhu, L. Y., & He, J. J. 2007, AJ, 134, 1475
Qian, S. B., Zhu, L. Y., Soonthornthum, B., et al. 2005, AJ, 130, 1206
Ricker, G. R., Winn, J. N., Vanderspek, R., et al. 2015, JATIS, 1, 1
Rousselot, P. 1984, BBSAG, 73
Ruciński, S. M. 1969, AcA, 19, 245
Ruciński, S. M. 1973, AcA, 23, 79
Ruciński, S. M. 1974, AcA, 24, 119
Rucinski, S. M. 1993, ASSL, 177, 111
Safar, J. 2003, BRKA
Shappee, B., Prieto, J. L., Grupe, D., & Shappee, B. 2014, ApJ, 788, 48
Tran, K., Levine, A., Rappaport, S., et al. 2013, ApJ, 774, 81
Van Hamme, W. 1993, AJ, 106, 2096
Weber, R. 1963, IBVS, 21
Wilson, R. E. 1979, ApJ, 234, 1054
Wilson, R. E. 1990, ApJ, 356, 613
Wilson, R. E., & Devinney, E. J. 1971, ApJ, 166, 605
Wilson, R. E., & Van Hamme, W. 2014, ApJ, 780, 151
Woźniak, P. R., Vestrand, W. T., Akerlof, C. W., et al. 2004, AJ, 127, 2436
Yakut, K., & Eggleton, P. P. 2005, ApJ, 629, 1055
Yang, Y. G., Qian, S. B., & Soonthornthum, B. 2012, AJ, 143, 122
Yang, Y. G., Qian, S. B., Zhang, L. Y., Dai, H. F., & Soonthornthum, B. 2013, AJ, 146, 35
Yang, Y. G., Qian, S. B., & Zhu, L. Y. 2005, AJ, 130, 2252
Yang, Y. G., Qian, S. B., Zhu, L. Y., & He, J. J. 2009, AJ, 138, 540
Zejda, M. 2004, IBVS, 5583
Zejda, M. 2006, JAVSO, 35, 211
Zhang, X. D., Qian, S. B., & Liao, W. P. 2020, MNRAS, 492, 4112
Zhu, L. Y., Qian, S. B., Soonthornthum, B., He, J. J., & Liu, L. 2011, AJ, 142, 124